RSC Advances

PAPER

Cite this: *RSC Adv.*, 2023, **13**, 8374

Facile preparation of nickel phosphide for enhancing the photoelectrochemical water splitting performance of $BiVO_4$ photoanodes†

Yongsheng Li,[a] Zhen Li,[bc] Chengwen Xu,[bc] Shuangwei Yu[bc] and Zijun Sun *[bc]

Received 17th January 2023
Accepted 7th March 2023

DOI: 10.1039/d3ra00346a

rsc.li/rsc-advances

The photoelectrochemical (PEC) water splitting performance of $BiVO_4$ (BVO), a promising photoanode material, is constrained by its extremely short hole diffusion length and slow water oxidation kinetics. Modification of oxygen evolution cocatalysts (OECs) by appropriate methods is a practical solution to enhance the PEC water splitting performance of BVO. In this work, two different nickel phosphides Ni_2P and $Ni_{12}P_5$ were prepared by a facile and mild one-step solvothermal method, and used as OECs to modify a BVO photoanode for enhancing the PEC water splitting performance. The BVO/Ni_2P and BVO/$Ni_{12}P_5$ photoanodes showed impressive photocurrent densities of 3.3 mA cm^{-2} and 3.1 mA cm^{-2}, respectively. In addition, the PEC water splitting stability of the BVO/Ni_2P photoanode was greatly enhanced compared to that of the bare BVO photoanode. Further characterization and photoelectrochemical analysis revealed that the significant improvement of the BVO photoanode performance was attributed to the effective inhibition of surface charge recombination, facilitation of interfacial charge transfer, and acceleration of water oxidation kinetics after Ni_2P and $Ni_{12}P_5$ modification.

Introduction

The development of renewable energy is a key initiative to curb global warming and combat climate change.[1] Various pathways for developing renewable energy have been investigated so far.[2–5] Among them, photoelectrochemical (PEC) water splitting, which converts solar energy into hydrogen, is considered an attractive candidate for the development of renewable energy sources.[6] PEC water splitting is composed of hydrogen evolution reaction (HER) and oxygen evolution reaction (OER),[7,8] and the latter one that occurred in the photoanode is considered to be a more challenging step because it involves four electron transfer, which is a complex thermodynamic "uphill" reaction that determines the efficiency of water splitting.[3] Therefore, the development of efficient photoanode materials is the key to achieving large-scale application for PEC water splitting. Photoanode materials are usually composed of n-type semiconductors (*e.g.* TiO_2,[9,10] Fe_2O_3,[11] WO_3,[12] $BiVO_4$,[13] Ta_3N_5 (ref. 14)). Among them, $BiVO_4$ (BVO) is considered as a potential photoanode material due to its abundant resources, suitable band gap, and highly oxidizing valence band position.[15,16] However, some physical and chemical properties of BVO limit its performance, mainly in terms of poor conductivity, short hole diffusion distance (2–4 nm), slow oxygen evolution kinetics, and severe photocorrosion.[17] Therefore, overcoming the inherent drawbacks of BVO to achieve high PEC performance remains a key challenge.

To overcome these advantages, many efforts, such as morphology control,[18] elemental doping,[19,20] construction of heterojunctions,[21,22] and modification of oxygen evolution cocatalysts (OECs),[23,24] have been adopted to improve the PEC performance of BVO-based photoanodes. In particular, modification of OECs on the photoanode surface is regarded as an effective strategy because it could suppress the surface charge recombination, promote the interfacial charge transfer and accelerate the water oxidation kinetics.[25,26] Therefore, modification of appropriate OECs plays a crucial role in PEC water splitting. In the last decade, a large number of metal inorganics have been used as OECs to improve the performance of photoanodes. In contrast to high-cost noble metal, the development of earth-abundant, cost-effective transition metal-based OECs is of more practical significance.[27,28] Recently, transition metal phosphides, which have been shown to have superior electrocatalytic OER performance than transition metal oxides/hydroxides,[29] were adopted to modify BVO photoanode as OECs for enhancing the PEC water splitting performance. Kim and coworkers used CoP to modify Mo doped BVO photoanodes, which achieved 2.5 mA cm^{-2} at 1.23 V_{RHE}.[30] Jiang *et al.* loaded

---

[a] *China Academy of Science & Technology Development GuangXi Branch, Nanning 530001, China*

[b] *School of Automation, Guangxi University of Science and Technology, Liuzhou 545006, China*

[c] *Guangxi Colleges and Universities Key Laboratory of Microwave Communication and Micro–Nano Photoelectric Technology, School of Electronic Engineering, Guangxi University of Science and Technology, Liuzhou 545006, China. E-mail: sunzijun@gxust.edu.cn*

† Electronic supplementary information (ESI) available. See DOI: https://doi.org/10.1039/d3ra00346a

CoP nanoparticles on the BVO surface to achieve a 2-fold increase in photocurrent at 1.23 V_{RHE},[31] and found that CoP could effectively promote surface charge separation. Ge and coworkers reported that loading FeP on BVO achieved a high photocurrent density of 3.05 mA cm^{-2} at 1.23 V_{RHE}.[32] These studies demonstrated the great potential of transition metal phosphides to enhance the PEC performance of BVO photoanodes. However, the reported studies mainly focused on cobalt phosphide, while nickel phosphide was rarely mentioned in PEC water splitting despite its superior OER activity.[33,34] In addition, the synthesis of metal phosphides in the above literature require a complex process of first preparing metal oxides or hydroxides and then converting the metal oxides or hydroxides to metal phosphides by phosphine gas released from $NaHPO_2$ under high temperature environment.[35] These high temperature oxygen-free conditions and at least two-step synthesis processes are not favorable for the application of metal phosphides.

Herein, nickel phosphides with different stoichiometry (Ni_2P and $Ni_{12}P_5$) were successfully synthesized by a facile and mild one-step solvothermal method, which were then used as OECs to modify BVO photoanodes for enhancing the PEC water splitting performance. The photocurrent densities of the BVO/Ni_2P and BVO/$Ni_{12}P_5$ photoanodes reached 3.3 mA cm^{-2} and 3.1 mA cm^{-2} at 1.23 V_{RHE}, respectively, which were much higher than that of bare BVO photoanode (1.4 mA cm^{-2} at 1.23 V_{RHE}). In addition, the stability of PEC water splitting was greatly enhanced of the BVO/Ni_2P photoanode compared with the bare BVO photoanode.

Experimental section

Materials

Bismuth nitrate pentahydrate ($Bi(NO_3)_3 \cdot 5H_2O$, 99%), dimethyl sulfoxide (DMSO, 99%), potassium iodide (KI, 99%), *p*-benzoquinone ($C_6H_4O_2$, 99%), vanadyl acetylacetonate ($VO(acac)_2$, 99%), nickel chloride hexahydrate ($NiCl_2 \cdot 6H_2O$, 99%), red phosphorus powder (P, 99%), ethylene glycol (EG, 99%) were purchased from Aladdin. FTO was purchased from Advanced Election Technology Co., Ltd, and rinsed with acetone, ethanol, and DI water before use.

Preparation of BVO/Ni_2P and BVO/$Ni_{12}P_5$ photoanodes

Porous BVO photoanode was synthesized based on previous literature.[36] Ni_2P and $Ni_{12}P_5$ were synthesized by a one-step solvothermal method. For the synthesis of Ni_2P, 200 mg $NiCl_2 \cdot 6H_2O$ was dissolved in 30 mL EG and stirred for 20 min, followed by the addition of 260 mg red phosphorus powder and stirred for another 20 min. Then transferred to a 50 mL Teflon-lined stainless-steel autoclave and heated at 190 °C for 12 h. After the autoclave cooled to room temperature, the black precipitate was collected by centrifugation, washed with ethanol and distilled water, and dried under vacuum. As for $Ni_{12}P_5$, the synthesis conditions were the same as Ni_2P except that the amount of red phosphorus powder was changed to 200 mg and the solution was changed to a mixture of 15 mL EG and 15 mL distilled water. To prepare BVO/Ni_2P and BVO/$Ni_{12}P_5$ photoanodes, 10 mg Ni_2P and $Ni_{12}P_5$ was dispersed in 1 mL ethanol and sonicated for 15 min to form a uniform suspension, respectively. Then 10 μL of suspension was drop-casted onto the BVO surface and dried at 60 °C for 30 min.

Characterization

The crystal structures were analyzed by X-ray diffraction analysis (XRD, Rigaku SmartLab). The chemical composition and elemental state of the material were analyzed by X-ray photoelectron spectroscopy (XPS, Thermo Scientific K-Alpha). The surface morphology and elemental distribution were analyzed by scanning electron microscopy (SEM, TESCAN MIRA LMS) equipped with an energy dispersive X-ray spectrometer (EDX). Prior to SEM measurements, samples were evaporated with Pt for 60 s. The optical properties were analyzed by UV-Vis spectroscopy (UV-Vis, PerkinElmer lambda950). Raman spectra were detected using the laser confocal micro Raman spectrometer (Raman, Zolix RTS2). High resolution transmission electron microscopy (HRTEM) images were detected on JEM-ARM200F field emission electron microscope.

Photoelectrochemical measurement

All photoelectrochemical measurements were tested in a standard three-electrode cell with an electrochemical workstation (CHI760E, Shanghai Chenhua Instrument Co., Ltd). The prepared photoanodes were used as the working electrode, Ag/AgCl (4 M KCl) as the reference electrode, Pt foil (1 cm × 1 cm) as the counter electrode, and 1 M KBi buffer (pH = 9) as the electrolyte. A 300 W xenon lamp (PLS-SEX300, Beijing Perfect Light Technology Co., Ltd) equipped with an AM 1.5G filter was used as the light source, and the incident light intensity was calibrated to 100 mW cm^{-2}. Linear sweep voltammogram (LSV) was scanned at a rate of 10 mV s^{-1}. Electrochemical impedance spectroscopy (EIS) was performed in the frequency range from 100 kHz to 0.1 Hz, and Mott–Schottky measurement was performed in the dark at a frequency of 1 kHz.

Results and discussion

The crystalline phase composition of the prepared samples was analyzed by XRD. Fig. 1a shows the XRD patterns of the bare BVO, BVO/Ni_2P, and BVO/$Ni_{12}P_5$ photoanodes. These photoanodes showed the similar diffraction peaks without any difference and all peaks are attributed to SnO_2 (PDF#46-1088) and $BiVO_4$ (PDF#75-1867), while no peaks belonging to Ni_2P and $Ni_{12}P_5$ were observed. To obtain the crystalline phase structures of the Ni_2P and $Ni_{12}P_5$ samples, powder XRD analysis was also performed (Fig. 1b). And the XRD patterns showed that the diffraction peaks of the samples match well with the hexagonal phase Ni_2P (PDF#74-1385) and tetragonal phase $Ni_{12}P_5$ (PDF#74-1381), respectively, demonstrating that the pure phase of Ni_2P and $Ni_{12}P_5$ were successfully synthesized. No peaks belonging to Ni_2P and $Ni_{12}P_5$ were observed in BVO/Ni_2P and BVO/$Ni_{12}P_5$ photoanodes was ascribed to the low content of

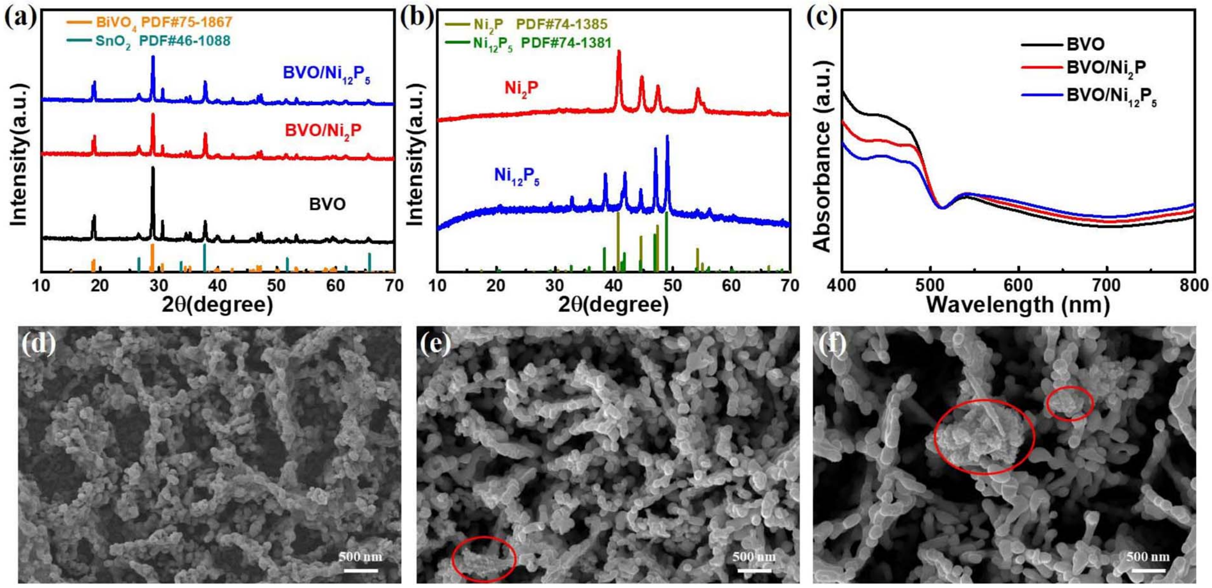

Fig. 1 XRD patterns of the (a) prepared photoanodes, (b) Ni_2P and $Ni_{12}P_5$. (c) UV-Vis spectra of the prepared photoanodes. SEM images of the (d) BVO, (e) BVO/Ni_2P, and (f) BVO/$Ni_{12}P_5$ photoanodes.

Ni_2P and $Ni_{12}P_5$. To explore the optical properties of the prepared photoanodes, the UV-Vis absorption spectra were also recorded (Fig. 1c). The absorption edge of the BVO was located at 513 nm, corresponding to a band gap value of 2.42 eV.[37] After the modification of Ni_2P and $Ni_{12}P_5$, the positions of the absorption edge were almost unchanged, indicating that Ni_2P and $Ni_{12}P_5$ didn't dope into the lattice and changed the band gap of the BVO. To further characterize the structure of the prepared photoanodes, the Raman spectroscopy was also performed (Fig. S1†). The Raman spectra showed that the characteristic peaks of the prepared photoanodes were almost identical and all correspond to monoclinic scheelite BVO,[38] and no peak of Ni_2P and $Ni_{12}P_5$ were observed, also suggesting the low content of Ni_2P and $Ni_{12}P_5$ dispersed on the BVO surface.

The morphologies of the prepared samples were investigated by SEM characterization. Fig. S2† shows the SEM images of Ni_2P and $Ni_{12}P_5$ samples. It was found that Ni_2P and $Ni_{12}P_5$ particles were aggregated without substrate, with Ni_2P tending to be flake-shaped while $Ni_{12}P_5$ tending to be rod-shaped. SEM image of the bare BVO was shown in Fig. 1d, which exhibited a porous dendritic morphology. After loading Ni_2P and $Ni_{12}P_5$, the morphologies still maintained the porous structure with some nanoparticles appearing on the surface marked by red circle (Fig. 1e and f). To prove the presence of Ni_2P and $Ni_{12}P_5$, EDX analysis were performed on BVO/Ni_2P and BVO/$Ni_{12}P_5$ photoanodes. The EDX results showed the existence of Ni, P, Bi, V, O, Sn, and C elements (Fig. S3a†). No other elements were observed except Sn element from FTO substrate and C element from conductive tape used for SEM characterization and adsorbed gaseous molecules.[32,39] In addition, the elemental mapping showed that Ni and P elements were mainly distributed in areas where the particles were aggregated (Fig. S3b†). The EDX analysis results of the BVO/$Ni_{12}P_5$ photoanode were similar to those of the BVO/Ni_2P photoanode (Fig. S4†). In order to clearly confirm the existence of Ni_2P and $Ni_{12}P_5$ in the prepared photoanodes, HRTEM was carried out. HRTEM images of BVO/Ni_2P exhibited lattice spacing of 0.22 nm and 0.31 nm, corresponding to the (111) plane of hexagonal Ni_2P and (112) plane of monoclinic BVO (Fig. 2a and b). As for BVO/$Ni_{12}P_5$, HRTEM images showed lattice spacing of 0.24 nm and 0.31 nm, corresponding to the (112) plane of tetragonal $Ni_{12}P_5$ and (112) plane of monoclinic BVO (Fig. 2c and d). These results further indicated the successful modification of Ni_2P and $Ni_{12}P_5$ on BVO photoanode.

XPS characterization was carried out to explore the elemental valence states of the prepared photoanodes. Fig. 3 shows the XPS spectra of BVO/Ni_2P and BVO/$Ni_{12}P_5$ photoanodes. The peaks (159.0 eV and 164.3 eV) shown in the Bi 4f spectrum (Fig. 3a) and the peak (516.5 eV) shown in V 2p spectrum (Fig. 3b) were attributed to Bi^{3+} and V^{5+} species, respectively, which match well with the monoclinic scheelite BVO.[40] For Ni 2p spectrum of BVO/Ni_2P (Fig. 3c), three groups of peaks at Ni $2p_{3/2}$ and Ni $2p_{1/2}$ were observed. One group of peaks at 853.0 eV and 870.3 eV corresponded to $Ni^{\delta+}$ species in Ni_2P, while the other two groups of peaks at 856.0 eV, 873.7 eV, 861.5 eV and 880.6 eV corresponded to the oxidized Ni^{2+} species and the satellite peak, respectively.[41] P 2p spectrum (Fig. 3d) displays two peaks at 129.6 eV and 133.2 eV, the former one is assigned to $P^{\delta-}$ species in Ni_2P and the latter one is attributed to surface nickel phosphate species due to exposure to air.[41–43] The Ni 2p spectrum and P 2p spectrum of BVO/$Ni_{12}P_5$ showed no significant differences compared to BVO/$Ni_{12}P_5$. It's worth noting that the $2p_{1/2}$ peak and $2p_{3/2}$ peak of $Ni^{\delta+}$ in BVO/Ni_2P sample were slightly higher than that in BVO/$Ni_{12}P_5$ by 0.1 eV and 0.2 eV, respectively, while $P^{\delta-}$ peak in BVO/Ni_2P sample was slightly lower than that in BVO/$Ni_{12}P_5$ by 0.1 eV, indicating that there is

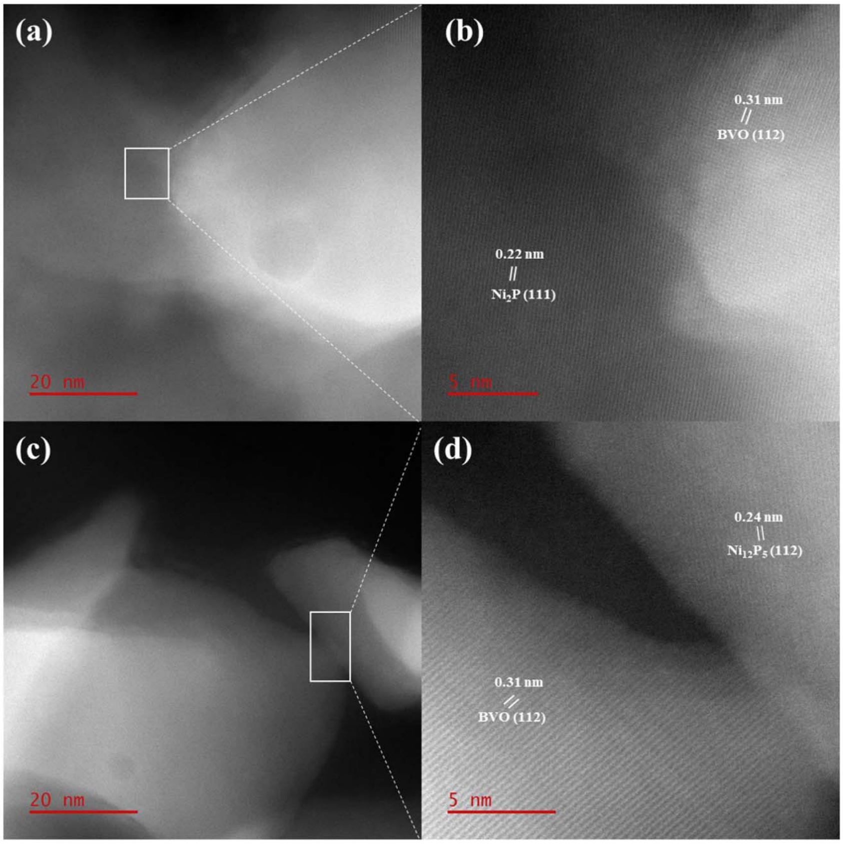

Fig. 2 HRTEM images of (a and b) BVO/Ni_2P, and (c and d) BVO/$Ni_{12}P_5$ photoanodes.

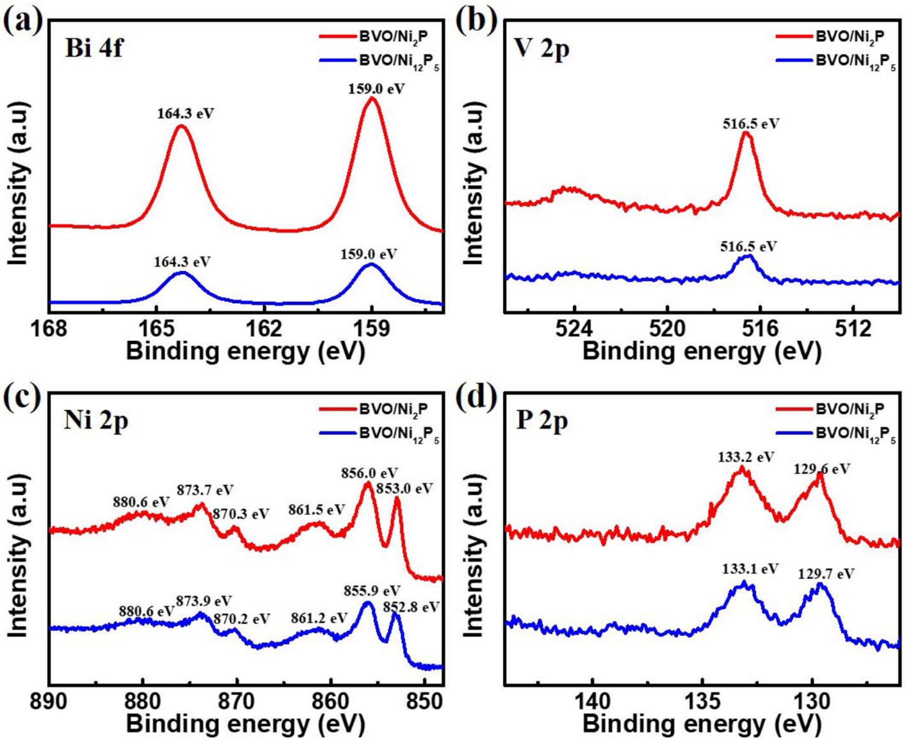

Fig. 3 XPS spectra of BVO/Ni_2P and BVO/$Ni_{12}P_5$ photoanodes. (a) Bi 4f, (b) V 2p, (c) Ni 2p, and (d) P 2p.

more electron transfer from Ni to P in Ni_2P due to the high P content compared to $Ni_{12}P_5$.[44,45]

To measure the PEC water splitting performance of the prepared photoanodes, LSV measurements were detected under illumination (AM 1.5G, 100 mW cm^{-2}). As shown in Fig. 4a, the photocurrent density of the bare BVO was 1.4 mA cm^{-2} at 1.23 V_{RHE}. After loading Ni_2P and $Ni_{12}P_5$, the photocurrent densities of the BVO/Ni_2P and BVO/$Ni_{12}P_5$ photoanodes increased significantly, indicating that the modification of Ni_2P and $Ni_{12}P_5$ could effectively improve the PEC water splitting performance of BVO. Notably, the BVO/Ni_2P photoanode showed a slightly higher photocurrent density (3.3 mA cm^{-2} at 1.23 V_{RHE}) than BVO/$Ni_{12}P_5$ photoanode (3.1 mA cm^{-2} at 1.23 V_{RHE}), reflecting that Ni_2P played a better role in enhancing the PEC water splitting performance. Fig. S5† shows the LSV curves of BVO/Ni_2P photoanode with different Ni_2P loading amounts. The photocurrent density increased significantly at only 2 μL Ni_2P loading, suggesting that Ni_2P could effectively enhance the PEC water splitting performance of the BVO photoanode. The optimal loading amount was 10 μL with a photocurrent density of 3.3 mA cm^{-2} at 1.23 V_{RHE}. LSV measurements without irradiation were also performed to evaluate the water oxidation kinetics. As shown in Fig. 4b, BVO/Ni_2P and BVO/$Ni_{12}P_5$ photoanodes showed much more negative onset potentials than bare BVO photoanode, indicating the faster water oxidation kinetics of BVO/Ni_2P and BVO/$Ni_{12}P_5$ photoanodes. Moreover, BVO/Ni_2P photoanode exhibited a more negative onset potential than BVO/$Ni_{12}P_5$ photoanode, reflecting that Ni_2P had higher catalytic water oxidation nature than $Ni_{12}P_5$. Fig. 4c shows the applied bias photon-to-current efficiency (APBE) of the prepared photoanodes. The maximum efficiency of bare BVO photoanode was 0.22% at 0.93 V_{RHE}, which was far inferior to those of BVO/Ni_2P and BVO/$Ni_{12}P_5$ photoanodes (0.93% at 0.71 V_{RHE} and 0.86% at 0.71 V_{RHE}, respectively). The lower potentials and higher efficiencies suggested that the BVO/Ni_2P and BVO/$Ni_{12}P_5$ photoanodes have superior PEC water splitting performance compared to bare BVO. The incident photon-to-current conversion efficiency (IPCE) is another key indicator for assessing the performance of photoanodes. As shown in Fig. 4d, all these photoanodes showed the best conversion efficiency under the irradiation of 400 nm wavelength, and the IPCE value of the BVO/Ni_2P photoanode reached 80%, which was much higher than those of the BVO/$Ni_{12}P_5$ (57%) and BVO (35%) photoanodes. This extremely high photon-to-current conversion efficiency illustrated that Ni_2P was a highly efficient OECs when modified on BVO. In order to evaluate the PEC stability of the prepared photoanodes, a long-term measurement was carried out (Fig. 4e and f). After 1 hour of PEC water splitting, the photocurrent density value of the bare BVO photoanode was decreased by 83% owing to severe photocorrosion. The stability of photoanodes was significantly improved after modification of Ni_2P and $Ni_{12}P_5$, with the photocurrent density values of BVO/Ni_2P and BVO/$Ni_{12}P_5$ decreased by 34% and 73%, respectively. It is noteworthy that BVO/Ni_2P exhibited better properties than BVO/$Ni_{12}P_5$, which could be ascribed to the stronger corrosion resistance with the higher P content of nickel phosphides.[46,47]

In order to investigate the charge separation process in PEC water splitting, LSV measurements were performed by adding Na_2SO_3 as a sacrificial agent to the electrolyte (Fig. S6†). Since the oxidation kinetics of Na_2SO_3 is much faster than that of water, holes can be consumed very quickly in the presence of Na_2SO_3. It could be clearly seen that there is a significant negative shift in the onset potential of the bare BVO photoanode

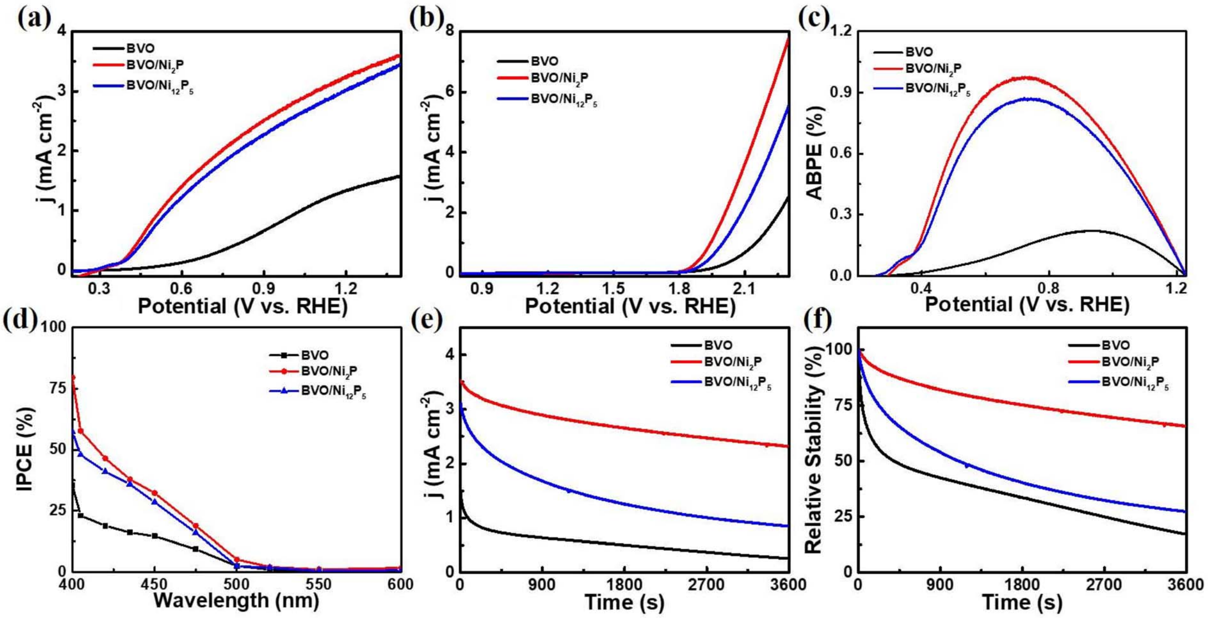

Fig. 4 LSV curves of the prepared photoanodes under (a) irradiation and (b) dark condition. (c) ABPE, (d) IPCE, and (e) j–t curves at 1.23 V_{RHE} of the prepared photoanodes. (f) On the basis of the data in (e), the calculated relative stability of the prepared photoanodes.

in the presence of Na_2SO_3, suggesting that the main factor for the poor water oxidation property of BVO was that the holes on the surface are highly susceptible to recombination. Notably, the BVO/Ni_2P and BVO/$Ni_{12}P_5$ photoanodes showed similar onset potentials as BVO photoanode in the presence of Na_2SO_3, suggesting that Ni_2P and $Ni_{12}P_5$ play a key role in suppressing the hole recombination on the surface and facilitating the hole transfer in the water oxidation process. The surface charge injection efficiency ($\eta_{\text{injection}}$) and the charge separation efficiency ($\eta_{\text{separation}}$) were calculated according to the formula $\eta_{\text{injection}} = j_{\text{water}}/j_{\text{sulfite}}$ and $\eta_{\text{separation}} = j_{\text{sulfite}}/j_{\text{abs}}$ with Na_2SO_3 as a sacrificial agent. The $\eta_{\text{injection}}$ of the BVO/Ni_2P and BVO/$Ni_{12}P_5$ photoanodes were 57% and 54% at 1.23 V_{RHE}, respectively, which were much higher than that of the bare BVO (25% at 1.23 V_{RHE}) photoanode (Fig. 5a), suggesting that the surface charges could be effectively transferred after modification of Ni_2P and $Ni_{12}P_5$. Fig. 5b shows $\eta_{\text{separation}}$ of the prepared photoanodes, $\eta_{\text{separation}}$ of the BVO/Ni_2P and BVO/$Ni_{12}P_5$ photoanodes showed slightly enhancements compared to BVO, indicating that the bulk charge transfer efficiency wasn't significantly enhanced by the modification of Ni_2P and $Ni_{12}P_5$. These results revealed that Ni_2P and $Ni_{12}P_5$ mainly play the role of suppressing the surface electron–hole pairs recombination and promoting surface hole transfer.

Transient photocurrent measurements were carried out to further explore the charge recombination process in PEC water splitting. Fig. 5c shows the transient photocurrent curves of the prepared photoanodes. All the photoanodes showed a sensitive response during the on/off irradiation switching. Once irradiation was turned on, the photocurrent curves showed an anodic photocurrent spike due to the instantaneous generation of photogenerated electron–hole pairs. Then, a decay of the

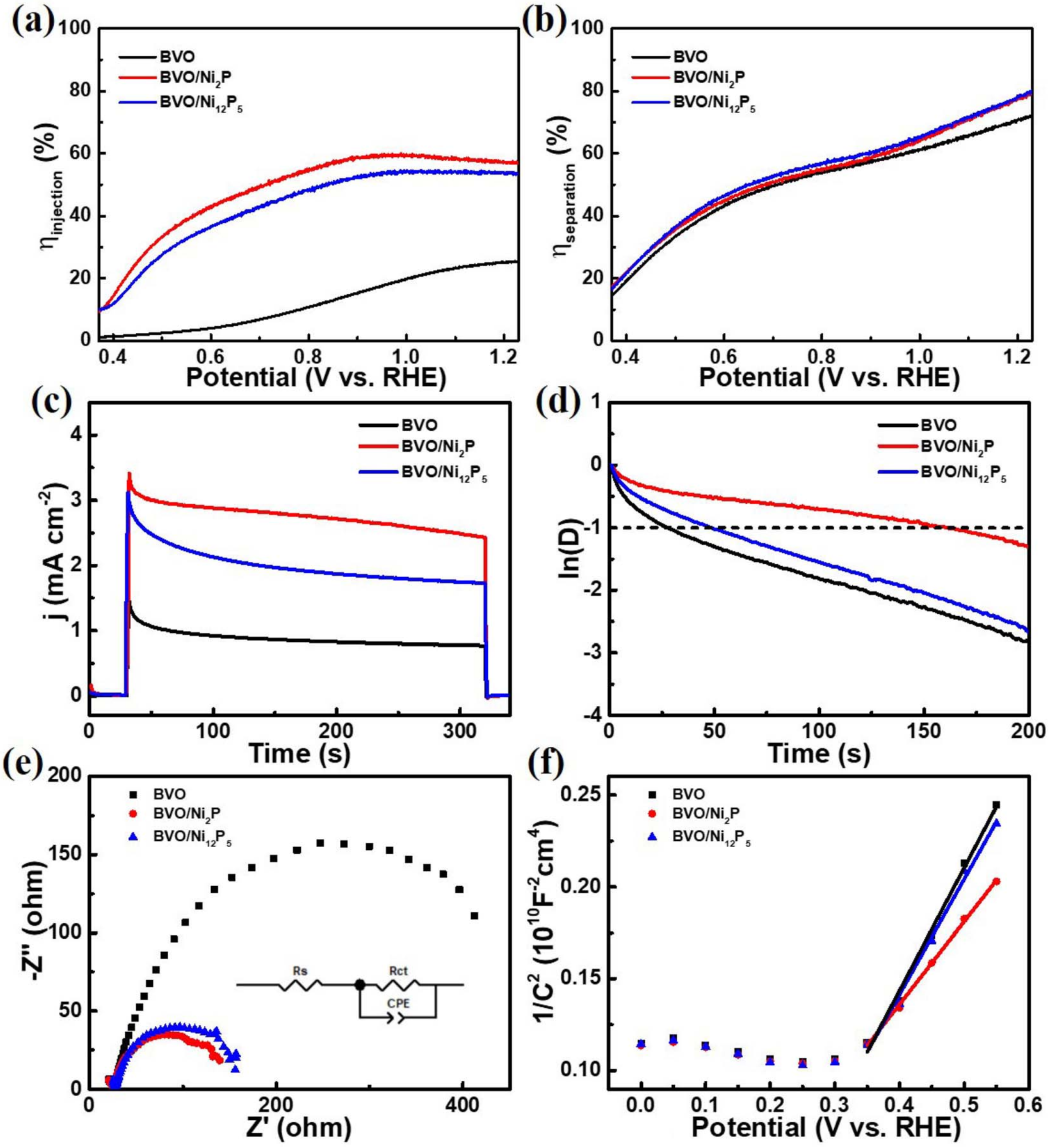

Fig. 5 (a) The calculated injection efficiency, (b) separation efficiency, (c) transient photocurrent at 1.23 V_{RHE}, (d) the calculated lifetime, (e) EIS Nyquist plots, and (f) M–S plots of the prepared photoanodes.

photocurrent caused by electron–hole recombination was immediately appeared until a stable photocurrent was reached. To quantify the electron–hole recombination behavior, the data in Fig. 5c were calculated. The transient time constant (τ) is defined as the time at $\ln D = -1$.[48] As shown in Fig. 5d, τ values were estimated to be 27 s, 161 s, 48 s for bare BVO, BVO/Ni_2P, and BVO/$Ni_{12}P_5$ photoanodes, respectively. After modification of Ni_2P and $Ni_{12}P_5$, the lifetime of photoanodes was effectively improved, and the BVO/Ni_2P photoanode showed a longer lifetime than BVO/$Ni_{12}P_5$ photoanode. The above results showed that Ni_2P was more effective in hindering the recombination of electron–hole pairs, which was attributed to more P-sites in Ni_2P due to the higher P content, and these P-sites could serve as the acceptor centers of charges to promote interfacial charges transfer.[44,45,49]

To further explore the role acted by nickel phosphide in PEC water splitting, electrochemical impedance spectroscopy (EIS) test was performed, and an appropriate EIS fitting model was employed based on the measured curves (Fig. 5e). R_s represented the contact resistance of the photoanode, while R_{ct} represented the interfacial charge transfer resistance.[50,51] The R_s values for the bare BVO, BVO/Ni_2P, and BVO/$Ni_{12}P_5$ photoanodes were 24.56 Ω, 22.72 Ω, 26.15 Ω, respectively. These very close R_s values indicated that the loading of Ni_2P and $Ni_{12}P_5$ didn't affect the photoanode contact. As for R_{ct}, the values of bare BVO, BVO/Ni_2P, and BVO/$Ni_{12}P_5$ photoanodes were 478.7 Ω, 127.3 Ω, 138.1 Ω, respectively. The R_{ct} value of the BVO photoanode was much larger than those of the BVO/Ni_2P and BVO/$Ni_{12}P_5$ photoanodes, suggesting that Ni_2P and $Ni_{12}P_5$ could significantly promote the interfacial charge transfer. Fig. 5f shows the Mott–Schottky measurements of the prepared photoanodes. Carrier density (N_d) values were calculated from the Mott–Schottky plots. The N_d values of the bare BVO, BVO/Ni_2P, and BVO/$Ni_{12}P_5$ photoanodes were estimated to be 3.11×10^{18} cm^{-3}, 4.61×10^{18} cm^{-3}, 3.31×10^{18} cm^{-3}, respectively. These similar N_d values reflected that the bulk charge separation of BVO hardly changed after the modification of Ni_2P and $Ni_{12}P_5$. Hence, the above results suggested that the Ni_2P and $Ni_{12}P_5$ mainly serve to inhibit the surface charge recombination, facilitate the interfacial charge transfer, and accelerate the water oxidation kinetics, which results in a significant improvement of the BVO photoanode performance. Moreover, owing to the higher P content of nickel phosphide, Ni_2P showed stronger corrosion resistant and more P-sites, leading to a better PEC water splitting performance compared to BVO/$Ni_{12}P_5$.

Conclusions

In summary, two different nickel phosphides Ni_2P and $Ni_{12}P_5$ were successfully prepared by a facile and mild one-step solvothermal method, and decorated on the BVO surface to construct BVO/Ni_2P and BVO/$Ni_{12}P_5$ composite photoanodes. PEC water splitting results showed that the photocurrent densities of BVO/Ni_2P and BVO/$Ni_{12}P_5$ photoanodes reached 3.3 mA cm^{-2} and 3.1 mA cm^{-2} at 1.23 V_{RHE}, respectively, which were much higher than that of the bare BVO photoanode. In addition, the stability of PEC water splitting was greatly enhanced for the BVO/Ni_2P photoanode compared to the bare BVO photoanode. Further investigations revealed that the significant improvement in performance was attributed to the effective inhibition of surface charge recombination, facilitation of interfacial charge transfer, and acceleration of water oxidation kinetics by Ni_2P and $Ni_{12}P_5$. These findings highlight the great potential of nickel phosphide in PEC water splitting and will provide an effective path for the design and fabrication of high performance photoanodes.

Conflicts of interest

The authors declare no conflicts of interest.

Acknowledgements

This work is financially supported by the National Natural Science Foundation of China (Grant No. 22269002), the Scientific Research Project of Guangxi University of Science and Technology's doctoral enterprise in Liuzhou (Grant No. BSGZ2131), the Science and Technology Project of Guangxi (Grant No. AD19110003), and the Doctoral Foundation of Guangxi University of Science and Technology (Grant No. 18Z12). The authors would like to thank Juncai Song from Shiyanjia Lab (**https://www.shiyanjia.com**) for the SEM characterization.

References

1 C. X. Hou, B. Wang, V. Murugadoss, S. Vupputuri, Y. F. Chao, Z. H. Guo, C. Y. Wang and W. Du, Recent advances in Co_3O_4 as anode materials for High-performance lithium-Ion batteries, *Eng. Sci.*, 2020, **11**, 19–30.

2 Y. P. Ma, X. B. Xie, W. Y. Yang, Z. P. Yu, X. Q. Sun, Y. P. Zhang, X. Y. Yang, H. Kimura, C. X. Hou, Z. H. Guo and W. Du, Recent advances in transition metal oxides with different dimensions as electrodes for high-performance supercapacitors, *Adv. Compos. Hybrid Mater.*, 2021, **4**, 906–924.

3 D. K. Lee, D. H. Lee, M. A. Lumley and K. S. Choi, Progress on ternary oxide-based photoanodes for use in photoelectrochemical cells for solar water splitting, *Chem. Soc. Rev.*, 2019, **48**, 2126–2157.

4 C. C. Dang, Q. Mu, X. B. Xie, X. Q. Sun, X. Y. Yang, Y. P. Zhang, S. Maganti, M. N. Huang, Q. L. Jiang, I. Seok, W. Du and C. X. Hou, Recent progress in cathode catalyst for nonaqueous lithium oxygen batteries: a review, *Adv. Compos. Hybrid Mater.*, 2022, **5**, 606–626.

5 Y. L. Zhao, F. Liu, K. J. Zhu, S. Maganti, Z. Y. Zhao and P. K. Bai, Three-dimensional printing of the copper sulfate hybrid composites for supercapacitor electrodes with ultra-high areal and volumetric capacitances, *Adv. Compos. Hybrid Mater.*, 2022, **5**, 1537–1547.

6 C. R. Jiang, S. J. A. Moniz, A. Q. Wang, T. Zhang and J. W. Tang, Photoelectrochemical devices for solar water splitting - materials and challenges, *Chem. Soc. Rev.*, 2017, **46**, 4645–4660.

7 X. C. Pan, Z. K. Zheng, X. L. Zhang, X. He, Y. S. An, Y. Hao, K. Huang and M. Lei, Multi-metallic nanosheets for high-performance hydrogen evolution reaction, *Eng. Sci.*, 2022, **19**, 253–261.

8 J. K. Zhao, K. Bao, M. Z. Xie, D. N. Wei, K. M. Yang, X. B. Zhang, C. Zhang, Z. L. Wang and X. J. Yang, Two-dimensional ultrathin networked CoP derived from $Co(OH)_2$ as efficient electrocatalyst for hydrogen evolution, *Adv. Compos. Hybrid Mater.*, 2022, **5**, 2421–2428.

9 M. Niu, K. Y. Sui, X. S. Wu, D. P. Cao and C. Z. Liu, GaAs quantum dot/TiO_2 heterojunction for visible-light photocatalytic hydrogen evolution: promotion of oxygen vacancy, *Adv. Compos. Hybrid Mater.*, 2022, **5**, 450–460.

10 M. L. Eqi, C. Shi, J. J. Xie, F. Y. Kang, H. J. Qi, X. S. Tan, Z. H. Huang, J. L. Liu and J. Guo, Synergetic effect of Ni-Au bimetal nanoparticles on urchin-like TiO_2 for hydrogen and arabinose co-production by glucose photoreforming, *Adv. Compos. Hybrid Mater.*, 2023, **6**, 5.

11 Z. J. Sun, G. S. Fang, J. L. Li, J. H. Mo, X. He, X. Wang and Z. Q. Yu, Preparation of (Ti, Zr) co-doped hematite photoanode for enhanced photoelectrochemical water splitting, *Chem. Phys. Lett.*, 2020, **754**, 137736.

12 X. Yin, W. X. Qiu, W. Z. Li, K. K. Wang, X. T. Yang, L. B. Du, Y. Liu and J. Li, Effects of alkali ion on boosting WO_3 photoelectrochemical performance by electrochemical doping, *Int. J. Hydrogen Energy*, 2020, **45**, 19257–19266.

13 Z. J. Sun, C. W. Xu, Z. Li, F. Guo, B. S. Liu, J. H. Liu, J. Zhou, Z. Q. Yu, X. He and D. C. Jiang, Construction of organic–inorganic hybrid photoanodes with metal phthalocyanine complexes to improve photoelectrochemical water splitting performance, *New J. Chem.*, 2022, **46**, 9111–9118.

14 Z. R. Lou, Y. C. Yang, Y. C. Wang, C. Qin, R. Liang, Y. W. Wang, Z. Z. Ye and L. P. Zhu, $LaCl_3$ flux mediated Ta_3N_5 planar photoanode for solar water oxidation, *Chem. Eng. J.*, 2020, **396**, 125161.

15 J. M. Wang, M. T. Kuo, P. Zeng, L. Xu, S. T. Chen and T. Y. Peng, Few-layer $BiVO_4$ nanosheets decorated with $SrTiO_3$: Rh nanoparticles for highly efficient visible-light-driven overall water splitting, *Appl. Catal., B*, 2020, **279**, 119377.

16 C. J. Xu, W. J. Sun, Y. J. Dong, C. Z. Dong, Q. Y. Hu, B. C. Ma and Y. Ding, A graphene oxide–molecular Cu porphyrin-integrated $BiVO_4$ photoanode for improved photoelectrochemical water oxidation performance, *J. Mater. Chem. A*, 2020, **8**, 4062–4072.

17 U. Prasad, J. Prakash, X. Shi, S. K. Sharma, X. H. Peng and A. M. Kannan, Role of alkali metal in $BiVO_4$ crystal structure for enhancing charge separation and diffusion length for photoelectrochemical water splitting, *ACS Appl. Mater. Interfaces*, 2020, **12**, 52808–52818.

18 T. S. Dabodiya, P. Selvarasu and A. V. Murugan, Tetragonal to monoclinic crystalline phases change of $BiVO_4$ *via* Microwave-Hydrothermal reaction: In correlation with Visible-Light-Driven photocatalytic performance, *Inorg. Chem.*, 2019, **58**, 5096–5110.

19 L. L. Wang, F. K. Wu, X. Y. Chen, J. Ren, X. Y. Lu, P. P. Yang and J. L. Xie, Defective Metal–Organic framework assisted with nitrogen doping enhances the photoelectrochemical performance of $BiVO_4$, *ACS Appl. Energy Mater.*, 2021, **4**, 13199–13207.

20 X. N. Jiang, S. Chen, X. R. Zhang, L. N. Qu, H. J. Qi, B. Wang, B. B. Xu and Z. H. Huang, Carbon-doped flower-like Bi_2WO_6 decorated carbon nanosphere nanocomposites with enhanced visible light photocatalytic degradation of tetracycline, *Adv. Compos. Hybrid Mater.*, 2023, **6**, 47.

21 Z. G. Guo, J. D. Wei, B. Zhang, M. N. Ruan and Z. F. Liu, Construction and photoelectrocatalytic performance of TiO_2/$BiVO_4$ heterojunction modified with cobalt phosphate, *J. Alloys Compd.*, 2020, **821**, 153225.

22 Y. N. Liu, C. Liu, C. L. Shi, W. Sun, X. Lin, W. L. Shi and Y. Z. Hong, Carbon-based quantum dots (QDs) modified ms/tz-$BiVO_4$ heterojunction with enhanced photocatalytic performance for water purification, *J. Alloys Compd.*, 2021, **881**, 160437.

23 G. Z. Fang, Z. F. Liu and C. C. Han, Enhancing the PEC water splitting performance of $BiVO_4$ co-modifying with NiFeOOH and Co-Pi double layer cocatalysts, *Appl. Surf. Sci.*, 2020, **515**, 146095.

24 H. D. She, P. F. Yue, J. W. Huang, L. Wang and Q. Z. Wang, One-step hydrothermal deposition of F:FeOOH onto $BiVO_4$ photoanode for enhanced water oxidation, *Chem. Eng. J.*, 2020, **392**, 123703.

25 X. T. Xu, L. Pan, X. Zhang, L. Wang and J. J. Zou, Rational design and construction of cocatalysts for semiconductor-based photo-electrochemical oxygen evolution: A comprehensive review, *Adv. Sci.*, 2019, **6**, 1801505.

26 R. Y. Wang, Z. Zhang, P. Du, Z. H. Fu, K. Huang, K. Xu, Y. X. Du, D. Y. Fan, R. Zhang and M. Lei, Efficient synthesis of sulfur-modified cobalt hydroxide self-supported electrocatalysts for enhanced oxygen evolution, *Adv. Compos. Hybrid Mater.*, 2022, **5**, 2491–2499.

27 W. Y. Yang, D. N. Peng, H. Kimura, X. Y. Zhang, X. Q. Sun, R. A. Pashameah, E. Alzahrani, B. Wang, Z. H. Guo, W. Du and C. X. Hou, Honeycomb-like nitrogen-doped porous carbon decorated with Co_3O_4 nanoparticles for superior electrochemical performance pseudo-capacitive lithium storage and supercapacitors, *Adv. Compos. Hybrid Mater.*, 2022, **5**, 3146–3157.

28 F. S. Li, Q. Y. Li, H. Kimura, X. B. Xie, X. Y. Zhang, N. N. Wu, X. Q. Sun, B. B. Xu, H. Algadi, R. A. Pashameah, A. K. Alanazi, E. Alzahrani, H. D. Li, W. Du, Z. H. Guo and C. X. Hou, Morphology controllable urchin-shaped bimetallic nickel-cobalt oxide/carbon composites with enhanced electromagnetic wave absorption performance, *J. Mater. Sci. Technol.*, 2022, **148**, 250–259.

29 A. Dutta and N. Pradhan, Developments of metal phosphides as efficient OER precatalysts, *J. Phys. Chem. Lett.*, 2017, **8**, 144–152.

30 J. H. Kim, S. H. Han, Y. H. Jo, Y. J. Bak and J. S. Lee, A precious metal-free solar water splitting cell with a bifunctional cobalt phosphide electrocatalyst and doubly promoted bismuth vanadate photoanode, *J. Mater. Chem. A*, 2018, **6**, 1266–1274.

31 D. C. Jiang, L. Zhang, Q. D. Yue, T. T. Wang, Q. Huang and P. W. Du, Efficient suppression of surface charge recombination by CoP-Modified nanoporous $BiVO_4$ for photoelectrochemical water splitting, *Int. J. Hydrogen Energy*, 2021, **46**, 15517–15525.

32 J. H. Ge, X. L. Ding, D. C. Jiang, L. Zhang and P. W. Du, Efficient improved charge separation of FeP decorated worm-like nanoporous $BiVO_4$ photoanodes for solar-driven water splitting, *Catal. Lett.*, 2020, **151**, 1231–1238.

33 M. M. Qian, S. S. Cui, D. C. Jiang, L. Zhang and P. W. Du, Highly efficient and stable water-oxidation electrocatalysis with a very low overpotential using FeNiP substitutional-solid-solution nanoplate arrays, *Adv. Mater.*, 2017, **29**, 1704075.

34 A. L. Han, H. L. Chen, Z. J. Sun, J. Xu and P. W. Du, High catalytic activity for water oxidation based on nanostructured nickel phosphide precursors, *Chem. Commun.*, 2015, **51**, 11626–11629.

35 Y. M. Zhang, L. Y. Liu, L. L. Zhao, C. X. Hou, M. N. Huang, H. Algadi, D. Y. Li, Q. Xia, J. Wang, Z. R. Zhou, X. Han, Y. X. Long, Y. B. Li, Z. D. Zhang and Y. Liu, Sandwich-like $CoMoP_2$/MoP heterostructures coupling N, P co-doped carbon nanosheets as advanced anodes for high-performance lithium-ion batteries, *Adv. Compos. Hybrid Mater.*, 2022, **5**, 2601–2610.

36 T. W. Kim and K. S. Choi, Nanoporous $BiVO_4$ photoanodes with dual-layer oxygen evolution catalysts for solar water splitting, *Science*, 2014, **343**, 990–994.

37 K. H. Ye, Z. S. Chai, J. W. Gu, X. Yu, C. X. Zhao, Y. M. Zhang and W. J. Mai, BiOI–$BiVO_4$ photoanodes with significantly improved solar water splitting capability: p–n junction to expand solar adsorption range and facilitate charge carrier dynamics, *Nano Energy*, 2015, **18**, 222–231.

38 K. Fan, H. Chen, B. W. He and J. G. Yu, Cobalt polyoxometalate on N-doped carbon layer to boost photoelectrochemical water oxidation of $BiVO_4$, *Chem. Eng. J.*, 2020, **392**, 123744.

39 S. Majumder, N. D. Quang, C. J. Kim and D. J. Kim, Anion exchange and successive ionic layer adsorption and reaction-assisted coating of $BiVO_4$ with Bi_2S_3 to produce nanostructured photoanode for enhanced photoelectrochemical water splitting, *J. Colloid Interface Sci.*, 2021, **585**, 72–84.

40 S. Q. Zhou, K. Y. Chen, J. W. Huang, L. Wang, M. Y. Zhang, B. Bai, H. Liu and Q. Z. Wang, Preparation of heterometallic CoNi-MOFs-modified $BiVO_4$: a steady photoanode for improved performance in photoelectrochemical water splitting, *Appl. Catal., B*, 2020, **266**, 118513.

41 X. Luo, R. Li, K. P. Homewood, X. X. Chen and Y. Gao, Hybrid 0D/2D Ni_2P quantum dot loaded TiO_2(B) nanosheet photothermal catalysts for enhanced hydrogen evolution, *Appl. Surf. Sci.*, 2020, **505**, 144099.

42 Z. J. Sun, H. F. Zheng, J. S. Li and P. W. Du, Extraordinarily efficient photocatalytic hydrogen evolution in water using semiconductor nanorods integrated with crystalline Ni_2P cocatalysts, *Energy Environ. Sci.*, 2015, **8**, 2668–2676.

43 Q. Mu, R. L. Liu, H. Kimura, J. C. Li, H. Y. Jiang, X. Y. Zhang, Z. P. Yu, X. Q. Sun, H. Algadi, Z. H. Guo, W. Du and C. X. Hou, Supramolecular self-assembly synthesis of hemoglobin-like amorphous CoP@N, P-doped carbon composites enable ultralong stable cycling under high-current density for lithium-ion battery anodes, *Adv. Compos. Hybrid Mater.*, 2023, **6**, 23.

44 Z. Q. Wang, L. F. Li, M. Z. Liu, T. F. Miao, X. J. Ye, S. G. Meng, S. F. Chen and X. L. Fu, A new phosphidation route for the synthesis of NiPx and their cocatalytic performances for photocatalytic hydrogen evolution over g-C_3N_4, *J. Energy Chem.*, 2020, **48**, 241–249.

45 Z. C. Sun, M. S. Zhu, M. Fujitsuka, A. J. Wang, C. Shi and T. Majima, Phase effect of NixPy hybridized with g-C3N4 for photocatalytic hydrogen generation, *ACS Appl. Mater. Interfaces*, 2017, **9**, 30583–30590.

46 A. E. Praveen, S. Ganguli, D. Sarkar and V. Mahalingam, Ligand-tuned energetics for the selective synthesis of Ni_2P and $Ni_{12}P_5$ possessing bifunctional electrocatalytic activity toward hydrogen evolution and hydrazine oxidation reactions, *Inorg. Chem.*, 2022, **61**, 4394–4403.

47 A. R. J. Kucernak and V. N. Naranammalpuram Sundaram, Nickel phosphide: the effect of phosphorus content on hydrogen evolution activity and corrosion resistance in acidic medium, *J. Mater. Chem. A*, 2014, **2**, 17435–17445.

48 X. B. Bu, Y. X. Gao, S. H. Zhang and Y. Tian, Amorphous cerium phosphate on P-doped Fe_2O_3 nanosheets for efficient photoelectrochemical water oxidation, *Chem. Eng. J.*, 2019, **355**, 910–919.

49 L. A. Stern, L. G. Feng, F. Song and X. L. Hu, Ni_2P as a Janus catalyst for water splitting: the oxygen evolution activity of Ni_2P nanoparticles, *Energy Environ. Sci.*, 2015, **8**, 2347–2351.

50 S. Majumder, N. D. Quang, T. T. Hien, N. D. Chinh, N. M. Hung, H. Yang, C. J. Kim and D. J. Kim, Effect of SILAR-anchored $ZnFe_2O_4$ on the $BiVO_4$ nanostructure: An attempt towards enhancing photoelectrochemical water splitting, *Appl. Surf. Sci.*, 2021, **546**, 149033.

51 C. X. Hou, W. Y. Yang, H. Kimura, X. B. Xie, X. Y. Zhang, X. Q. Sun, Z. P. Yu, X. Y. Yang, Y. P. Zhang, B. Wang, B. B. Xu, D. Sridhar, H. Algadi, Z. H. Guo and W. Du, Boosted lithium storage performance by local build-in electric field derived by oxygen vacancies in 3D holey N-doped carbon structure decorated with molybdenum dioxide, *J. Mater. Sci. Technol.*, 2023, **142**, 185–195.